JOURNAL OF MATERIALS SCIENCE 9 (1974) 29–40

Direct observation of grain-boundary dislocations in the FeCo alloy

Part 1 *Theoretical observations*

M. J. MARCINKOWSKI, WEN FENG TSENG*, E. S. DWARAKADASA†
Engineering Materials Group, and Department of Mechanical Engineering, University of Maryland, College Park, Maryland, USA

A unified dislocation theory of grain boundaries proposed earlier for simple cubic crystals has been extended to include the case of ordered and disordered body-centred-cubic structures. Pure symmetric and asymmetric tilt and pure twist boundaries have been treated in detail and extended to an arbitrary grain boundary. It is shown that a unique set of coincidence site lattices exists for both the symmetric and asymmetric boundaries and that each of these sets, in turn, depends upon the rotation axis which characterizes the boundary. Furthermore, a unique set of grain-boundary dislocations is associated with each of these coincidence site lattices. The results are then applied to the transmission electron microscopy studies carried out in Part 2 of the present study.

1. Introduction

A generalized theory of grain boundaries has been proposed earlier whereby the grain-boundary structure can be described as being comprised of various combinations of crystal lattice dislocations (CLD) associated with the two adjacent grains [1]. This dislocation theory of grain boundaries was next extended to both symmetric [2] and asymmetric [3] tilt boundaries, as well as to twist boundaries [4] in both ordered and disordered simple cubic (sc) structures. The purpose of the present manuscript is to extend this analysis to that of a real crystal, in particular, the body-centred-cubic (bcc) lattice and its ordered counterpart, the CsCl structure. These results will then be compared with experimental findings obtained with both the ordered and disordered FeCo alloy using transmission electron microscopy techniques.

2. Symmetric tilt boundaries

In earlier studies [2-4] the rotation axes Ω associated with the grain boundaries were all chosen as [100], i.e. the four-fold symmetry axis. This can also be done for the bcc lattice as shown in Fig. 1 where it will be noted that two distinct layers of atoms comprise the atom configuration. Unlike the case of the simple cubic lattice where the Burgers vector was $a_0\langle 100\rangle$, it is now $a_0/2\langle 111\rangle$ for the bcc crystal. The grain boundary shown in Fig. 1 is one of symmetric tilt type of angular misorientation 53.1° and is a primary coincidence site boundary. This can be verified by first considering the following relation:

$$\tan \theta/2 = \frac{N b_x}{M d_y} \cdot \qquad (1)$$

In the above equation, b_x is the component of a single CLD or combination thereof along the x-axis in either grain while d_y is the spacing between planes along the y direction in either grain. N and M are simply integers and represent physically the number of single CLD or combinations thereof associated with a given plane and the number of interplanar spacings between these CLD, respectively. The CLD are shown to occur in pairs at the grain boundary in Fig. 1 each of which is derived from one of the two

*Now with The Department of Mechanical Engineering, University of Delaware, Newark, Delaware, USA.
†On leave from The Materials Research Group, Department of Metallurgy, Indian Institute of Science, Bangalore – 560012, India.

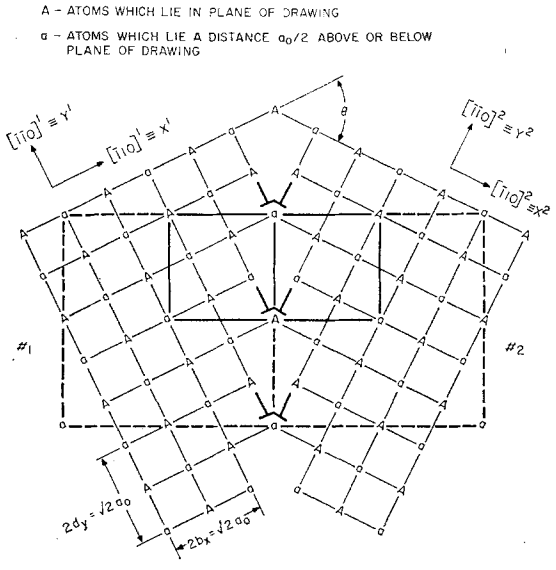

Figure 1 Symmetric high angle tilt boundary with primary coincidence angle $\theta_c{}^P = 53.1°$ in a body-centred-cubic lattice. Rotation axis is [001] and is normal to the drawing.

grains. Each CLD pair may be visualized as a grain-boundary dislocation (GBD) [2] of magnitude given by

$$b_{GB} = 2\,b_x \cos\theta/2\,. \tag{2}$$

It is apparent that b_x in Equation 1 represents only the edge portion of the single CLD or CLD combination and has no component of the Burgers vector which lies in the plane of the boundary. The screw components associated with the CLD from adjacent grains as well as the edge components with Burgers vector that lie in the plane of the boundary must be such that they cancel one another in order that no long range stresses be generated at the boundary. With the above considerations in mind, b_x may be expressed as follows:

$$b_x = b_{xz}\,\frac{Hh + Kk + Ll}{\sqrt{(H^2 + K^2 + L^2)}\,\sqrt{(h^2 + k^2 + l^2)}} \tag{3}$$

where b_{xz} is the magnitude of the Burgers vector, and the subscript xz emphasizes that the Burgers vector itself must lie in the xz plane. The quantity b_{xz} may be associated with a single CLD or combination thereof such that it possesses no component along the y-axis, while h, k, l are the indices associated with the Burgers vector of this dislocation and H, K, L are the indices associated with the x^1 or x^2 directions. It is important to note that the b_{xz} associated with the dislocation from each grain must be such that their z components cancel. The interplanar spacing d_y is given simply by

$$d_y = \frac{a_0}{\sqrt{(h_p{}^2 + k_p{}^2 + l_p{}^2)}} \tag{4}$$

where h_p, k_p, l_p are the indices pertaining to the slip plane associated with b_x. Combining Equations 1, 3 and 4

$$\tan\theta/2 = \frac{N\,b_{xz}}{M\,a_0}\,\sqrt{(h_p{}^2 + k_p{}^2 + l_p{}^2)}\;\frac{Hh + Kk + Ll}{\sqrt{(H^2 + K^2 + L^2)}\,\sqrt{(h^2 + k^2 + l^2)}}\,. \tag{5}$$

Equation 5 is just the coincidence site relation, similar to that given by $\tan\theta/2 = N/M$, for a sc crystal with rotation axis $\langle 100\rangle$ [2]. In the present case, however, Equation 5 represents the coincidence site relation for a bcc crystal of arbitrary rotation axis.

Equation 5 is most readily applied to the case shown in Fig. 1 by referring to the [001] standard projection shown in Fig. 2. From this figure it is apparent that the GBD can comprise single CLD with Burgers vectors given by $\frac{1}{2}\,a_0\,[\bar{1}\,1\,1]$. Thus, the values of h, k and l are $\bar{1}\,1\,1$ whereas, that of b_{xz} is $\sqrt{3}\,a_0/2$ while those of H, K and L are $\bar{1}\,1\,0$ and h_p, k_p and l_p are $\bar{1}\,\bar{1}\,0$. Upon substitution of these quantities into Equation 5, the following relation obtains:

$$\tan\theta/2\;\Big|\;\frac{(\bar{1}\,1\,0)}{[0\,0\,1]} = \frac{N}{M} \tag{6}$$

where the subscript [001] corresponds to the rotation axis associated with the tilt boundary, while the superscript $(\bar{1}\,1\,0)$ designates the mirror plane of the boundary defined with respect to the original perfect crystal or equivalently the mean $(\bar{1}\,1\,0)$ plane associated with both grains comprising the grain boundary. This relation is exactly the same as that obtained for the sc crystal. Equation 6 also holds for face-centred-cubic (fcc) crystals and has been used as the basis for the analysis of GBD in gold [5, 6]. More specifically, reference to Fig. 1 shows that $N = 1$ while $M = 2$. A primary coincidence site boundary corresponds to $N = 1$ [4]. It is also important to note that in order that the screw components cancel, the Burgers vector of the CLD associated with grain no. 1 must be $\frac{1}{2}\,a_0\,[\bar{1}\,1\,1]$, while that in grain no. 2 must be $\frac{1}{2}\,a_0\,[\bar{1}\,1\,\bar{1}]$. Still another requirement that must be met in the choice of b_x and d_y in Equation 1 for

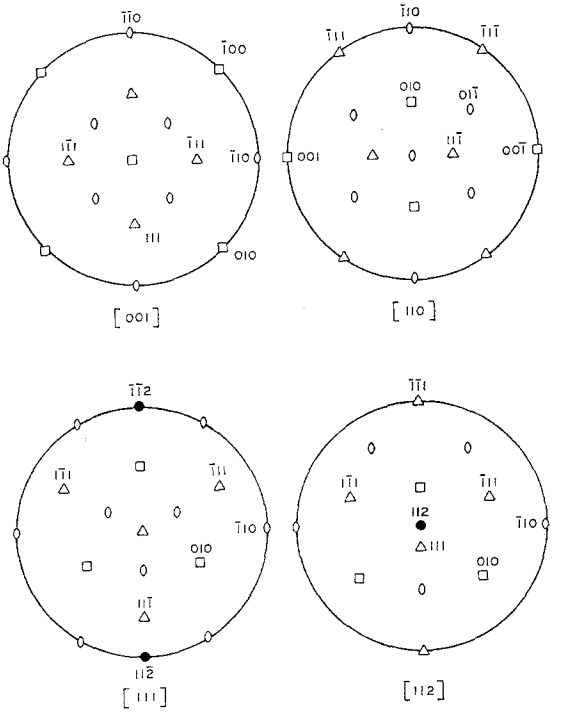

Figure 2 Standard projections associated with a cubic crystal for the orientations indicated.

a given grain-boundary rotation axis is that the crystal must possess a mirror plane passing through both the rotation axis and the slip plane normal. For example, in the case just considered, the rotation axis was [001] and the normal to the slip plane was $[\bar{1}\,\bar{1}\,0]$, both of which lie in, and thus define, the $(\bar{1}\,1\,0)$ mirror plane, as can be readily seen by reference to Fig. 2. It is apparent from this definition that all poles associated with permissible mirror planes will lie on the great circles representing the planes of projection in Fig. 2.

Reference to Fig. 2 shows that a second distinct type of mirror plane exists for the [001] standard projection which passes through both [001] and [010]. The y-axis can thus be chosen along $[0\,\bar{1}\,0]$ and the x-axis along $[\bar{1}\,0\,0]$. On the other hand, unlike the previous mirror plane, the Burgers vectors associated with the new mirror plane in Fig. 2 have components along both the y- and z-axes. Both the y and z components of the Burgers vector in grain no. 1 can be eliminated by combining the dislocation pair with Burgers vector $\frac{1}{2}\,a_0[\bar{1}\,1\,1]$ and $\frac{1}{2}\,a_0\,[\bar{1}\,\bar{1}\,\bar{1}]$ to give a resulting dislocation with Burgers vector $a_0\,[\bar{1}\,0\,0]$. A similar dislocation can be made in grain no. 2. It follows that h, k and l are given by $\bar{1}\,0\,0$ whereas $b_{xz} = b_x = a_0$ while H, K and L are $\bar{1}\,0\,0$ and h_p, k_p and l_p are 0 2 0. It is important to note that values of h_p, k_p and l_p are chosen commensurate with the smallest interplanar spacing since it is possible for the CLD combination given by $a_0\,[\bar{1}\,0\,0]$ to be associated with any of these planes. From Equations 3 and 4 it thus follows that $b_x = a_0$ while $d_y = a_0/2$, respectively, which leads to the following relation:

$$\tan\theta/2 \left| \frac{(\bar{1}\,0\,0)}{[0\,0\,1]} = \frac{2N}{M} \right. . \qquad (7)$$

It is apparent that the above relation differs from that of Equation 6. The meaning of this difference can be seen by referring to Fig. 3 in which $N = 1$ and $M = 4$ which as in the case of Fig. 1 again produces a 53.1° symmetric tilt boundary. However, the present grain boundary defined in terms of the above values of $b_x = a_0$ and $d_y = a_0/2$ is markedly different from the boundary shown in Fig. 1 corresponding to $b_x = \sqrt{2}\,a_0/2$ and $d_y = \sqrt{2}\,a_0/2$. In particular, large gaps are left within the grain boundary of Fig. 3. These gaps may be eliminated, however, by visualizing each dislocation component b_x which comprises the grain-boundary dislocation to be split into halves of magnitude $b_x/2$ as shown by

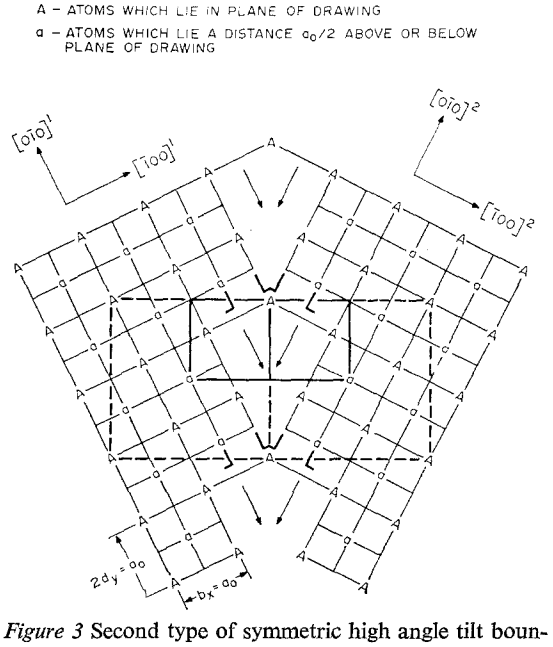

Figure 3 Second type of symmetric high angle tilt boundary with primary coincidence angle $\theta_c^P = 53.1°$ in a body-centred-cubic lattice. Rotation axis is [001] and is normal to the drawing.

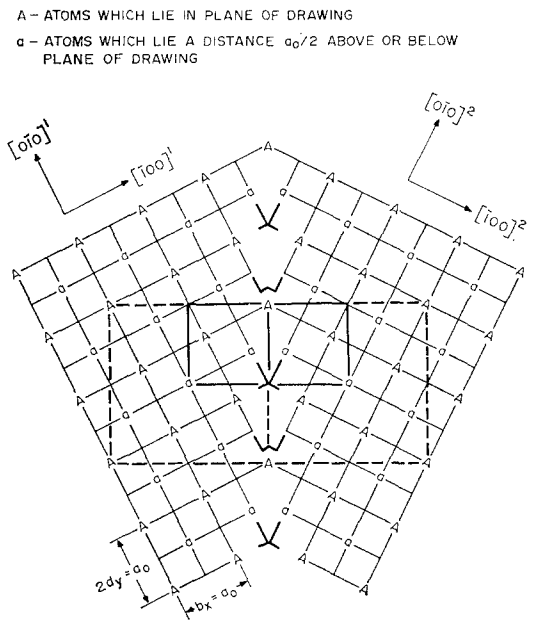

Figure 4 Same boundary as that shown in Fig. 3 but after the grain-boundary dislocations have dissociated into partials by climb.

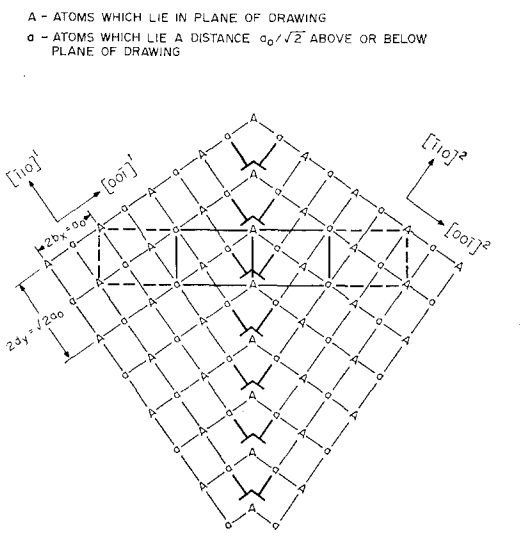

Figure 5 Symmetric high angle tilt boundary with primary coincidence angle $\theta_c^P = 70.5°$ in a body-centred-cubic lattice. Rotation axis is [110] and is normal to the drawing.

the normal and reversed L symbols in Fig. 3. These half dislocations can then be visualized as undergoing downward climb, as shown by the arrows in Fig. 3, resulting in the final grain-boundary configuration shown in Fig. 4. The resulting grain-boundary configuration can then be visualized as being comprised of half GBD each of magnitude $b_{GB}/2$. A similar type of climb process has been invoked previously to show the relationship between primary and secondary coincidence angle boundaries [2]. In summary then, two distinct types of reference axis exist for the [001] rotation axes which can be used to describe two unique types of symmetric tilt boundary and these reference axes are oriented 45° with respect to one another. Further significance will be associated with these two types of axes in the discussion of symmetric twist boundaries which will follow later.

Equation 5 can next be applied to the case of a symmetric tilt boundary with a [110] rotation axis by referring to the standard [110] projection shown in Fig. 2. As in the case of the [001] rotation axis discussed previously, two distinct types of symmetric grain boundary can be described. In the first case h, k and l are chosen as $11\bar{1}$ while $b_{xz} = \sqrt{3}\, a_0/2$, whereas H, K and L are $00\bar{1}$ and h_p, k_p and l_p are given by $\bar{1}10$ so that Equation 5 becomes

$$\tan\theta/2 \left| \frac{(00\bar{1})}{[110]} = \frac{N}{M}\frac{\sqrt{2}}{2} \right. . \qquad (8)$$

The above trigonometric function also applies for fcc and sc crystals. Fig. 5 shows a primary symmetric tilt boundary given by Equation 6 where $N = 1$ and $M = 1$ leading to a misorientation angle $\theta_c^P = 70.5°$ where the superscript P refers to primary and the subscript c refers to coincidence site lattice. The coincidence site lattice concept will be discussed in detail shortly.

Reference to Fig. 2 shows that a second mirror plane exists for the [110] standard projection which passes through both [110] and [001]. The y-axis can thus be chosen along [001] and the x-axis along $[\bar{1}10]$. However, the Burgers vectors of the CLD associated with the new mirror plane in Fig. 2 have components along the y-axis. In order to eliminate these components, it is necessary to obtain b_x by combining a pair of CLD such as $\frac{1}{2}\, a_0\, [\bar{1}1\bar{1}]$ and $\frac{1}{2}\, a_0\, [\bar{1}11]$ within each of the two adjacent grains to give a net Burgers vector equal to $a_0\, [\bar{1}10]$. Note that this resultant dislocation has no screw components, i.e. no component of the Burgers vector along the z direction. In order to determine the coincidence site lattice relationship, it follows from the above discussion that h, k and l equals $\bar{1}10$, the corresponding value of $b_{xz} = b_x = \sqrt{2}\, a_0$, while H, K and L

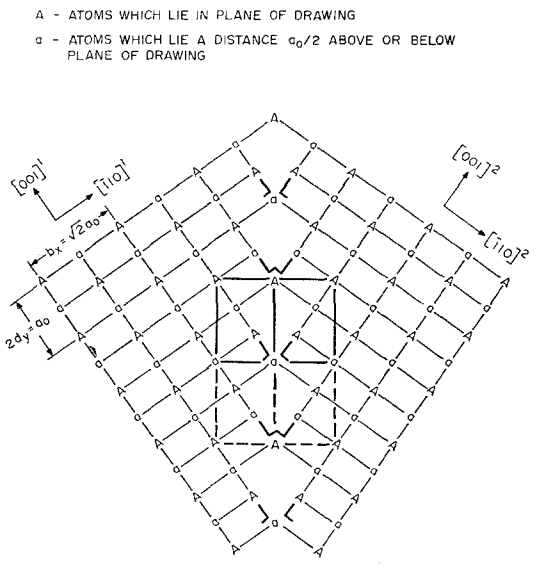

Figure 6 Second representation of high angle tilt boundary with primary coincidence angle $\theta_c^P = 70.5°$ in a body-centred-cubic lattice. Rotation axis is [110] and is normal to the drawing.

equals $\bar{1}10$ and h_p, k_p and l_p equals 002 which gives

$$\tan\theta/2 \left| \frac{(\bar{1}10)}{[110]} = \frac{N}{M} 2\sqrt{2} \right. . \qquad (9)$$

As expected from the results obtained for a [001] rotation axis, the two distinct mirror planes associated with the [110] rotation axis give rise to two different coincidence site boundary relationships. The difference between the two can again be seen by referring to Fig. 6 which, as in the case of Fig. 5, is also a primary coincidence site angle but with $N = 1$ and $M = 4$. Following the procedure employed for Fig. 4, the GBD illustrated in Fig. 6 are shown dissociated into half GBD in order that the large voids that would otherwise be present in the boundary are eliminated.

Equation 5 employed in conjunction with the [111] standard projection shown in Fig. 2 can also be used to determine the coincidence site lattice orientations associated with the symmetric tilt boundaries in which the rotation axes are [111]. There are two mirror planes associated with the [111] tilt axis given by $(\bar{1}10)$ and $(\bar{1}\bar{1}2)$. Consider first $(\bar{1}10)$. From Fig. 2 CLD of type $\frac{1}{2}a_0$ $[\bar{1}11]$ and $\frac{1}{2}a_0$ $[\bar{1}1\bar{1}]$ within each grain can be combined to give a_0 $[\bar{1}10]$. It follows, therefore, that h, k and l are given by $\bar{1}10$ while $b_{xz} = b_x = \sqrt{2}a$ and H, K and L are $\bar{1}10$ while h_p, k_p and l_p equal $\bar{1}\bar{1}2$ so that $d_y = a_0/\sqrt{6}$ and Equation 5 becomes

$$\tan\theta/2 \left| \frac{(\bar{1}10)}{[111]} = \frac{N2\sqrt{3}}{M} \right. . \qquad (10)$$

Fig. 7 shows a symmetric tilt boundary corresponding to Equation 10 in which $N = 1$ and $M = 4$ giving $\theta_c^P = 81.8°$. Again, as in Figs. 4 and 6 the GBD associated with Fig. 7 are seen to have dissociated into half GBD.

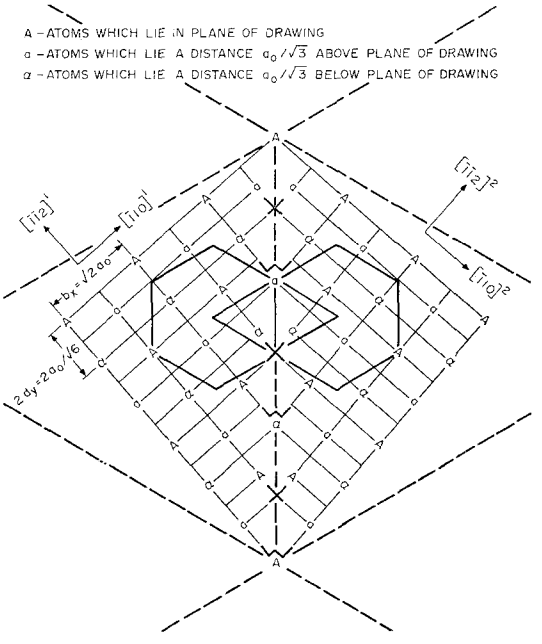

Figure 7 Symmetric angle tilt boundary with primary coincidence angle $\theta_c^P = 81.8°$ in a body-centred-cubic lattice. Rotation axis is [111] and is normal to the drawing.

The second coincidence site lattice angle relation associated with the [111] rotation axis in Fig. 2 is based upon the $(\bar{1}\bar{1}2)$ mirror plane. For this particular situation b_{xz} is obtained by combining the two CLD given by $\frac{1}{2}a_0$ $[\bar{1}11]$ and $\frac{1}{2}a_0$ $[1\bar{1}1]$ to obtain a_0 [001] or else using the single CLD $\frac{1}{2}a_0$ $[11\bar{1}]$. In either case they lead to the following coincidence site angle relation:

$$\tan\theta/2 \left| \frac{(\bar{1}\bar{1}2)}{[111]} = \frac{N2\sqrt{3}}{M3} \right. . \qquad (11)$$

Realizing that b_x associated with the above relation is equal to $2a_0/\sqrt{6}$, inspection of Fig. 7 shows that symmetric tilt boundaries based upon Equation 11 will also be comprised of half GBD.

Finally, Fig. 2 shows the standard [112]

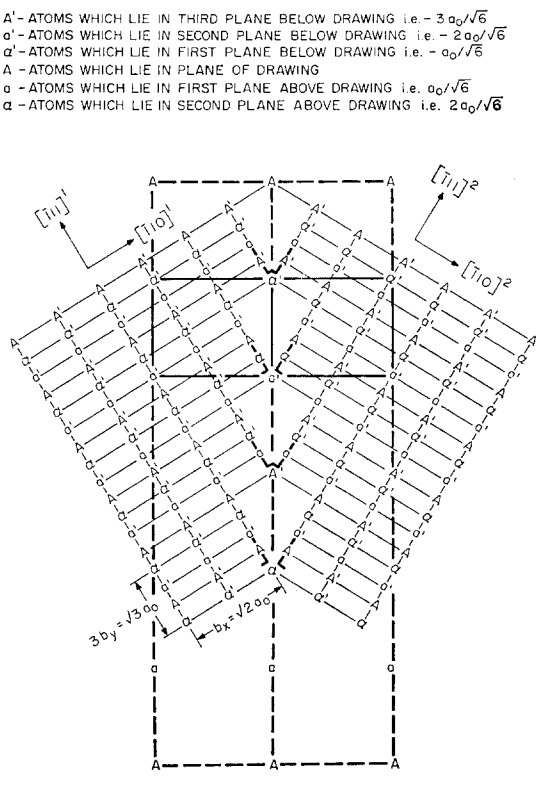

Figure 8 Symmetric high angle tilt boundary with primary coincidence angle $\theta_c^P = 62.8°$ in a body-centred-cubic lattice. Rotation axis is [112].

projection which again can be seen to possess two mirror planes, i.e. $(\bar{1}10)$ and $(\bar{1}\bar{1}1)$. Using the procedures discussed earlier, the coincidence site angle relation associated with the first of these mirror planes is readily found to be given by

$$\tan \theta/2 \left| \frac{(\bar{1}10)}{[112]} \right. = \frac{N}{M}\sqrt{6} \qquad (12)$$

while $b_x = \sqrt{2}\, a_0$ and $d_y = \sqrt{3}\, a_0/3$. Fig. 8 shows a primary symmetric tilt boundary based upon Equation 12 where $N = 1$ and $M = 8$ leading to $\theta_c^P = 62.8°$. Here again, the grain boundary is seen to be composed of half GBD, since two extra half planes are associated with $b_x = \sqrt{2}\, a_0$.

For the second $(\bar{1}\bar{1}1)$ mirror plane associated with the [112] rotation axis in Fig. 2, the coincidence site angle is found to be identical to that given by Equation 12 but with $b_x = \sqrt{3}\, a_0$ and $d_y = \sqrt{2}\, a_0/2$. Since reference to Fig. 8 shows that three extra half planes are associated with $b_x = \sqrt{3}\, a_0$, the symmetric tilt boundary corresponding to the $(\bar{1}\bar{1}1)$ mirror plane will be comprised of one-third GBD.

A symmetric tilt boundary of any rotation axis can, therefore, be constructed by employing the above procedures. It is to be emphasized that any grain boundary can be formed by suitable combinations of CLD and this provides the basis upon which the present analysis rests. One of the implications of this treatment is that the grain boundary may increase or decrease its angle θ only by having whole GBD with Burgers vectors given by Equation 2 either form or dissociate at the grain boundary, respectively. In the latter case, if the GBD are one-half or one-third etc GBD, they must first combine by climb since only the full GBD can dissociate into an integral number of GBD.

2.1. The coincidence site lattice

References to Figs. 1 and 3–8 all show that each of the symmetric tilt boundaries possess a common unit cell. In fact, two distinct types of unit cell may be defined. On the one hand, there is a coincidence site lattice with respect to the projection of atoms or sites normal to the plane of the drawing. The coincidence site lattice site unit cells for this case are shown in heavy outline. On the other hand, the true coincidence site lattices, where the atoms do in fact coincide in space, are shown by the dashed line extensions of the previously defined projection type coincidence site lattices. It is apparent that the true coincidence site lattice unit cells are significantly larger than the projection type unit cells. On the other hand, because of their smaller size, it is somewhat more convenient to use the smaller unit cells and this procedure will be followed throughout the remainder of the present study. The grain boundary is seen to be coincident with one of the edges of the coincidence site lattice unit cells. Furthermore, each of the unit cells reflects the symmetry of the rotation axes, i.e. four-fold, two-fold and three-fold in Figs. 1, 3, 4 and 5, 6, 8 and 7, respectively. The coincidence site lattice unit cell can be discussed in detail by reference to Fig. 9 which shows the unit cell corresponding to the 70.5° boundary illustrated in Fig. 5. The coincidence site lattice unit cell edges are readily found to be

$$b_{0c} = \sqrt{[(Nb_x)^2 + (Md_y)^2]} \qquad (13a)$$

and

$$a_{0c} = b_{0c}/\tan(\theta/2) = b_{0c}/(Nb_x/Md_y). \qquad (13b)$$

In those cases where more than one extra half

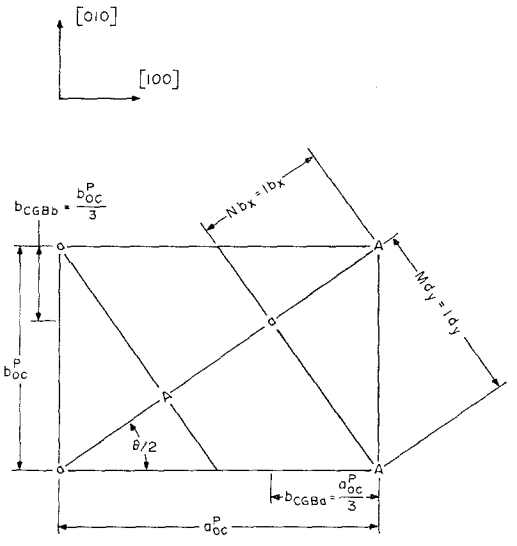

Figure 9 Unit cell of primary coincidence site lattice shown in Fig. 5 for $\theta_c{}^P = 70.5$.

plane is associated with b_x, i.e. when the GBD decompose into half GBD as in Figs. 3, 4 and 6–8, b_{0c} and a_{0c} must be divided by the appropriate integer which represents the degree of GBD dissociation, e.g. 2 in the case of the above-mentioned figures. For the coincidence site lattice unit cells shown in Figs. 1, 3, 4 and 7, the unit cell edges are all equal to b_{0c}. Note in particular in Fig. 7 that the unit cells have been drawn both as equilateral triangles, as well as hexagons. Both representations display the proper symmetry of the boundary, but from space filling arguments, the latter is perhaps more useful. Also evident from Fig. 9 is that two distinct Burgers vectors may be associated with the smallest interplanar spacings, namely $b_{CGBa} = a_{0c}{}^P/[N^2 + 2M] = a_{0c}{}^P/3$ and $b_{CGBb} = b_{0c}{}^P/[N^2 + 2M] = b_{0c}{}^P/3$ where the subscript CGBb signifies the closest interplanar spacing associated with the coincidence site lattice unit cell along the b-axis. The magnitude of $b_{0c}{}^P$ in Fig. 9 is also equal to the spacing between GBD, either whole or partial. The above relationships could also be used in conjunction with Fig. 6 but with the roles of N and M interchanged.

2.2. Primary and secondary GBD

Two slip systems may be associated with each of the individual grains comprising the coincidence site boundaries shown in Figs. 1 and 3–8. A primary system is defined by planes with interplanar spacing d_y whose normals lie along the y direction and by Burgers vectors which lie along the x direction and possess a value of b_x. In fact, all of the boundaries discussed thus far have been derived from CLD associated with the primary slip systems, i.e. $N = 1$ in Equation 1. On the other hand, a secondary slip system can be defined in which the slip plane normals lie along x while the Burgers vectors lie along the y direction. Appropriate values of d_x and b_y similar to those given by Equations 4 and 3, respectively, can be used for the secondary slip system by use of Fig. 2. In fact, the secondary slip system of Fig. 5 is just the primary slip system of Fig. 6 and vice versa. Having defined a primary and a secondary slip system, any grain boundary can be described in terms of some suitable combination of both [1, 2]. In addition, any equilibrium boundary, i.e. one containing no long range stresses, can always be defined in terms of a coincidence site lattice. Also, for any coincidence site lattice reference to Fig. 9 shows that two basic types of GBD may be defined as follows:

$$\mathbf{b}_{GBX} = 2\,b_x \cos\theta/2\,[100] = 2b_x \frac{Md_y}{\sqrt{[(Nb_x)^2 + (Md_y)^2]}}\,[100] \tag{14a}$$

$$\mathbf{b}_{GBY} = 2b_x \sin\theta/2\,[010] = 2b_x \frac{Nb_x}{\sqrt{[(Nb_x)^2 + (Md_y)^2]}}\,[010]. \tag{14b}$$

Equation 14a can be used to define the GBD which characterize the symmetric tilt component of the grain boundary while Equation 14b can be related to the asymmetric component of the grain boundary. Depending upon whether b_x corresponds to a single or multiple extra half plane, the Burgers vectors given by the above equations will correspond to full or partial GBD, respectively. In fact, if the GBD given by Equations 10 are full, then they are simply combinations of pairs of CLD from adjacent grains on the primary slip planes which can be expressed as

$$\mathbf{b}_{GB} = \mathbf{b}_{x_1} \pm \mathbf{b}_{x_2} \tag{15}$$

where the plus sign pertains to Equation 14a while the minus sign refers to Equation 14b. The quantities $\mathbf{b}_{x_1}$ and $\mathbf{b}_{x_2}$ are simply the vector components of CLD or combinations thereof

resolved along the x directions in grains no. 1 and 2, respectively.

2.3. Effect of atomic ordering on the coincidence site lattice

Another interesting aspect of coincidence site lattices is the effect of atomic ordering thereon. Assuming a CsCl type equiatomic AB type superlattice, it is apparent from Fig. 1 that A atoms lie at A sites whereas B atoms lie at a sites. It can be seen from this figure that when $N + M$ is odd, atomic ordering doubles the size of the coincidence site lattice unit cell. When $N = M$ and is even, on the other hand, atomic ordering leaves the coincidence site lattice unit cell unaffected. These are the same results that were obtained for the case of the sc lattice [2] where the grain-boundary rotation vector was along [001]. For a [110] rotation axis, the situation is somewhat different. In the particular case shown in Fig. 5, atomic ordering leads to a doubling of the b-axis of the coincidence site lattice unit cell when N is odd but leaves the length of the a-axis unchanged. In the case of Fig. 6, on the other hand, atomic ordering does not affect the length of the b-axis but does lead to a doubling of the a-axis when M is odd. It follows, then, that each specific type of grain boundary must be analysed separately in order to discern the effect of atomic ordering upon it. Of course, when the true coincidence site lattice unit cell illustrated by the dashed lines is chosen, the rules must again be modified. In particular, atomic ordering has no effect on the true coincidence site lattice unit cell shown in Fig. 1 since for such unit cells $M + N$ is always even.

3. Twist boundaries

Having discussed the principles associated with symmetric tilt boundaries, it is a simple matter to extend them to symmetric twist boundaries. In particular, Fig. 10 shows the twist analogue of the 70.5° tilt boundary shown in Fig. 5. Here again, a coincidence site lattice can be defined which is identical to that for the tilt boundary. However, unlike the case of the symmetric tilt boundary where only one side of the coincidence site lattice unit cell was coincident with the grain-boundary plane, all four sides of the unit cell now lie in the grain-boundary plane. In addition, it has been shown, using a simple cubic lattice, that the sides of the coincidence site lattice unit cells are coincident with GBD [4]. Note that for the symmetric tilt boundary, the

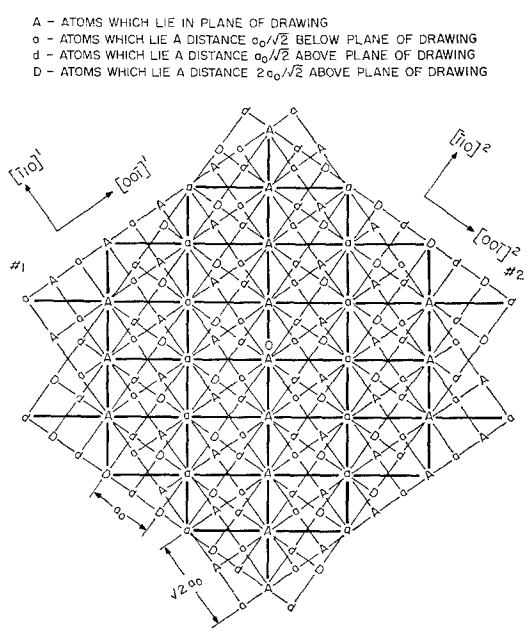

Figure 10 Symmetric high angle twist boundary with primary coincidence angle $\theta_c^P = 70.5°$ in a body-centred-cubic lattice. Rotation axis is [110] and is normal to the drawing.

GBD are coincident with the corners of the coincidence site lattice unit cell. It is also apparent from inspection of Figs. 5 and 6 that the horizontal array of GBD in Fig. 10 are full GBD while the GBD comprising the vertical array are half GBD. This is easily seen by noting that the vertical GBD pass alternately through all A sites or all a sites; i.e. every half period. Furthermore these GBD shown in Fig. 10 can be visualized as being formed by the combination of one cross-grid of screw type CLD from grain no. 1 with a corresponding cross grid from grain no. 2 according to the reaction given by Equation 15 with a plus sign. With these modifications in mind, all of the relations given earlier for the symmetric tilt boundary hold for the symmetric twist boundary. The GBD associated with a twist boundary will reflect the symmetry of the twist axis in that they will form a square array for the [001] twist axis, i.e. four-fold symmetry, a rectangular array for the [110] twist axis as in Fig. 10, i.e. two-fold symmetry, and an equilateral triangular array for the [111] twist axis, i.e. three-fold symmetry. Another interesting feature of the two-fold [110] twist axis in Fig. 10 is that it reflects simultaneously the mirror

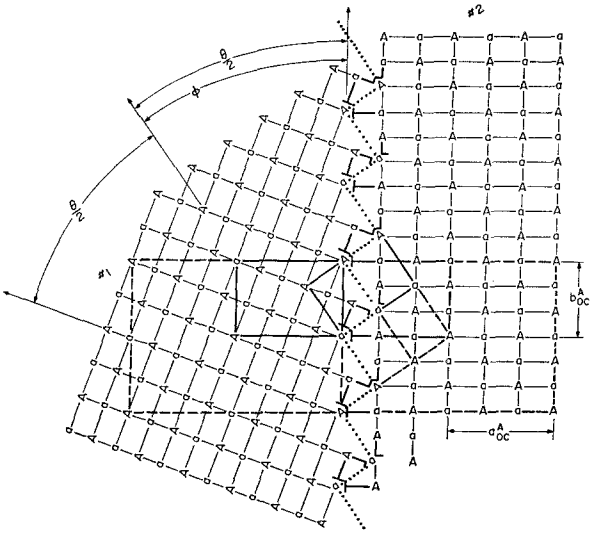

Figure 11 Asymmetric high angle tilt boundary with $\theta_c{}^P = 70.5°$ and $\phi = 35.25°$ in a body-centred-cubic lattice as shown in Fig. 6.

symmetry possessed by the tilt boundary in Fig. 5 and that in Fig. 6. In particular, the symmetry shown in Fig. 6 can be arrived at in Fig. 10 by a 90° rotation about the twist axis. Similar relations can be obtained for different rotation axes.

4. Asymmetric tilt boundaries

It is now possible to extend the previous arguments pertaining to symmetric boundaries to asymmetric ones as has already been done for sc crystals [3]. Consider for example, the case of the 70.5° symmetric boundary in Fig. 6 which is made asymmetric as shown by the dotted line in Fig. 11. The asymmetry is measured by the angle ϕ, i.e. the angle that the mean boundary direction makes with the original symmetric boundary. In accordance with the discussions relating to Figs. 5 and 6, the grain boundary in Fig. 11 is seen to comprise of equal numbers of full and half GBD. It is immediately apparent that the asymmetric tilt boundary has associated with it its own unique coincidence site lattice and will be termed the asymmetric coincidence site lattice to distinguish it from the symmetric coincidence site lattice which is also outlined in Fig. 11. As in the case of the symmetric boundary, there are two ways in which the unit cell associated with the asymmetric coincidence site lattice can be described. It may be formulated in terms of the smaller unit cell outlined by heavy solid lines in Fig. 11 associated with atom coincidence with respect to projection on the plane of the drawing, or it may be described in terms of the true spatial atom coincidence where the unit cell is outlined by heavy dashed lines. Again, for convenience the smaller coincidence site lattice unit cell will be employed in the following discussion, where the unit edges are designated by $a_{0c}{}^A$ and $b_{0c}{}^A$.

The asymmetric boundary shown in Fig. 11 can be visualized as being derived from the symmetric one shown in Fig. 6 by passing CLD pairs of strength N' on the secondary slip planes of grain no. 1 at slip plane intervals given by M' on the secondary slip plane spacings. In the specific case shown in Fig. 11 it is apparent that $N' = 1$ and $M' = 2$. In general, one may write

$$\tan(\theta/2 + \phi) = \frac{N' b_y}{M' d_x} \cdot \qquad (16)$$

The above expression is simply the coincidence relationship for asymmetric tilt boundaries similar to that given by Equation 1 for symmetric tilt boundaries. Again, as in the case of Equation 1 since N' and M' are discrete and since θ is fixed by Equation 1, ϕ must possess discrete values, i.e. it cannot be a continuous variable. Thus, for each θ there is a set of values for ϕ. It is also obvious from Fig. 11 that when $\phi = \pi/2$ the asymmetric tilt boundary is converted to a

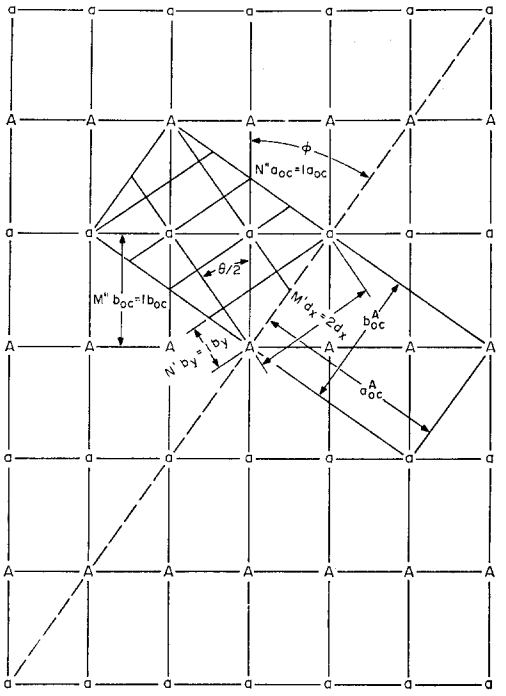

Figure 12 Relationship between crystal lattice, symmetric coincidence site lattice and asymmetric coincidence site lattice.

new symmetric tilt boundary of the type shown in Fig. 5.

It is also possible to describe the asymmetric coincidence site lattice unit cell of the asymmetric tilt boundary in terms of the symmetric coincidence site lattice unit cell of the symmetric tilt boundary. This can be most readily seen by reference to Fig. 12 which represents the same boundary as that shown in Fig. 11. From this figure it follows that

$$\tan\phi = \frac{N'' a_{0c}}{M'' b_{0c}} \tag{17}$$

where N'' corresponds to an integral number of unit cell lengths of the type a_{0c} while M'' corresponds to the number of unit cell lengths of the type b_{0c}. In the case of Fig. 12, both N'' and M'' are equal to unity. It also follows that

$$b_{0c}{}^{A} = \sqrt{[(N'' a_{0c})^2 + (M'' b_{0c})^2]} \tag{18a}$$

and

$$a_{0c}{}^{A} = b_{0c}{}^{A}/\tan\phi = b_{0c}{}^{A}/(N'' a_{0c}/M'' b_{0c}) \tag{18b}$$

which are relations similar to those given by Equation 13a and b for the symmetric coincidence site lattice unit cells. It is also interesting to note that the asymmetric coincidence site lattice unit cells also possess the same symmetry as does the symmetric coincidence site lattice unit cells. If the bcc lattice orders to the CsCl type superlattice configuration then it follows from inspection of Fig. 11 that the small asymmetric coincidence site lattice is doubled along both edges when N' is odd and is left unchanged when N' is even. These results are somewhat different from those obtained for the symmetric coincidence site lattice unit cells shown in Figs. 5 and 6 where atomic ordering doubled only one of the small unit cell edges of the disordered structure.

It is also possible to define twist boundaries with tilt components by allowing a pure symmetric twist boundary such as that shown in Fig. 10 to rotate about any axis which lies in the plane of the boundary. As in the case of the asymmetric tilt boundary, a set of discrete boundaries, but of mixed type, will be generated by this kind of operation. These particular types of twist boundaries have been treated in greater detail separately [7].

5. General grain boundaries

Having developed a detailed analysis of both symmetric tilt and twist and asymmetric tilt boundaries, it is a relatively simple matter to extend these concepts to a general grain boundary using the method of Bishop and Chalmers [8]. In particular, Fig. 13a shows a completely closed grain-boundary surface with rectangular faces. The top and bottom faces of the surface are comprised of pure symmetric twist type boundaries while the four side faces are of pure asymmetric tilt type. For conveniences, the twist axis Ω has been chosen parallel to [001] as in Figs. 1, 3 and 4 although it could easily have been chosen as any other axis such as [110], [111] or [112] as in Figs. 5 and 6, and 7 and 8, respectively. From the standard grain-boundary surface shown in Fig. 13a, in which the coincidence site lattice unit cell edges $a_{0c}{}^{P}$ and $b_{0c}{}^{P}$ may be made to coincide with the two sets of GBD in the cross grid, it is possible to represent a grain boundary of any selected orientation. In particular, Fig. 13b shows an asymmetric tilt boundary obtained by first making an oblique cut parallel to the rotation axis and then allowing the dislocations on the top and bottom faces to become continuous with one another across this new cut surface. In a similar manner, the two twist boundaries with tilt components shown in Figs. 13c and d can easily be generated along

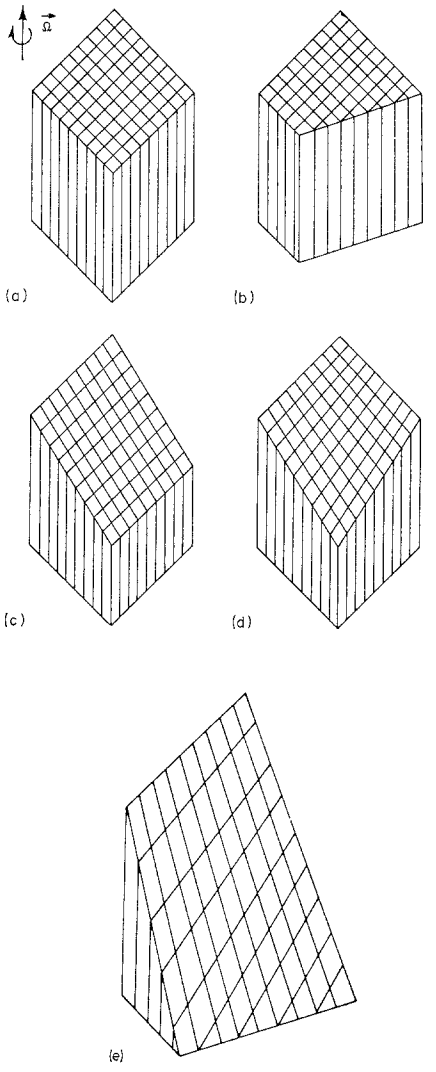

Figure 13 (a) Three-dimensional grain-boundary surface comprised of symmetric tilt and twist boundaries from which (b) asymmetric tilt (c) and (d) asymmetric twist boundaries can be generated. (e) Arbitrary grain boundary generated from Fig. 13a.

with the more generalized grain boundary shown in Fig. 13e. Inspection of the various GBD configurations in Fig 13 shows that in general, the GBD will neither be parallel nor orthogonal to one another.

All of the grain boundaries discussed thus far have been of the equilibrium or low energy type; that is, they possessed no long range stress fields. However, during the process of grain-boundary migration, such as occurs during grain growth or during plastic deformation, high internal stresses may be associated with the grain boundary. These internal stresses may arise from the presence of GBD, and/or wedge disclination dipoles and have been treated in detail elsewhere [1, 3, 9–11]. These particular defects will again be more appropriately considered in Part 2 of the present study. In concluding this section, it is to be emphasized that the present treatment of grain boundaries, although similar in many respects to that of Bollmann [12], is based almost exclusively on a dislocation approach. In particular, the present treatment starts from the premise that any grain boundary can be described in terms of a suitable combination of CLD from the two adjacent grains. The differences and similarities of the two approaches have been detailed in earlier studies [2, 3].

6. Summary and conclusions

A unified theory of grain boundaries based upon a dislocation approach which was originally developed for simple cubic lattices has been extended to bcc and the related CsCl type ordered lattices. In particular, both symmetric tilt and twist boundaries, as well as asymmetric tilt boundaries, have been treated for any number of different rotation axes. It is then shown how these results can be extended to boundaries of general type. A well-defined coincidence site lattice is found to be associated with both the symmetric as well as the asymmetric grain boundaries. Furthermore, a unique set of grain-boundary dislocations is, in turn, associated with each of the coincidence site lattices. The motivation for the present studies was to understand the transmission electron microscopy study of grain boundaries to be presented in the following paper.

Acknowledgements

The authors would like to express their appreciation to Dr K. Sadananda of The Engineering Materials Group and The Department of Mechanical Engineering of The University of Maryland for numerous enlightening discussions during the course of this investigation. In addition, they would also like to express their appreciation to the anonymous reviewer of the present manuscript for a number of very helpful comments. The present study was supported by the National Science Foundation under Grant No. GH-32262.

References

1. M. J. MARCINKOWSKI and E. S. P. DAS, *Phil. Mag.* **26** (1972) 1281.
2. M. J. MARCINKOWSKI, K. SADANANDA and WENG FENG TSENG, *Phys. Stat. Sol.* **17a** (1973) 423.
3. M. J. MARCINKOWSKI and K. SADANANDA, *ibid* **18a** (1973) 361.
4. M. J. MARCINKOWSKI and E. S. DWARAKADASA, *ibid*, **19a** (1973).
5. T. SCHOBER and R. W. BALLUFFI, *ibid* **644** (1971) 103, 115.
6. *Idem*, *Phil. Mag.* **21** (1970) 109.
7. E. S. DWARAKADASA and M. J. MARCINKOWSKI, to be submitted for possible publication.
8. G. H. BISHOP and B. CHALMERS, *Phil. Mag.* **24** (1971) 515.
9. E. S. P. DAS and M. J. MARCINKOWSKI, *J. Mat. Sci. and Eng.* **8** (1971) 189.
10. *Idem*, *Acta Metallurgica* **20** (1972) 199.
11. M. J. MARCINKOWSKI, E. S. P. DAS and K. SADANANDA, *Phys. Stat. Sol.* **19a** (1973) 67.
12. W. BOLLMANN, "Crystal Defects and Crystalline Interfaces" (Springer-Verlag, Berlin, 1970).

Received 4 June and accepted 26 July 1973.